

Ion partitioning at the oil–water interface as a source of tunable electrostatic effects in emulsions with colloids

Mirjam E. Leunissen,^{†*a} Jos Zwanikken,^{*b} René van Roij,^{*b} Paul M. Chaikin^{†*c}
and Alfons van Blaaderen^{*a}

Received 24th July 2007, Accepted 21st September 2007

First published as an Advance Article on the web 5th October 2007

DOI: 10.1039/b711300e

We present a combined experimental and theoretical investigation of the surprisingly strong electrostatic effects that can occur in mixtures of low- and high-polar liquids (*e.g.* oil–water emulsions), here in the presence of colloidal particles. For our experiments, we used confocal microscopy imaging, supplemented with electrophoresis and conductivity measurements. Theoretically, we studied our systems by means of a modified Poisson–Boltzmann theory, which takes into account image charge effects and the electrostatic self-energies of the micro-ions in the different dielectric media. Our results show that the unequal partitioning of micro-ions between the two liquid phases is the common driving force behind most of the observed electrostatic effects. The structural signatures of these effects typically develop on a time scale of hours to days and are qualitatively well-described by our theory. We demonstrate how the partitioning process and its associated phenomena can be controlled by shifting the balance of the interlocked ionic dissociation and partitioning equilibria. Moreover, we present strong experimental proof that the two-dimensional colloidal crystals at the oil–water interface are due to long-ranged Coulombic repulsion through the oil phase. The acquired insight in the role of electrostatics in oil–water emulsions is important for understanding the interactions in particle-stabilized (‘Pickering’) and charge-stabilized emulsions, emulsion production, encapsulation and self-assembly.

Introduction

Both oil–water emulsions, with small droplets of one liquid suspended in the other, and solid particle suspensions are ubiquitous in nature and industry. The stabilization of these emulsions and colloidal particle suspensions against phase separation and aggregation is an ancient problem of great importance. Whereas ‘emulsifiers’, for instance surfactants and small particles, are commonly used to prepare stable oil–water mixtures, solid colloids are often stabilized by a charge on their surface.^{1–4}

Naturally, it is expected that charges are important for the particle interactions in high dielectric constant (ϵ) liquids, such as water ($\epsilon_{\text{water}} \approx 80$), because there the energetic penalty for charge separation is small. Lately, however, the focus has shifted to lower dielectric constant media, in which electrostatics can also play a surprisingly dominant role.^{5–11} Especially the ‘low-polar’ regime ($5 \lesssim \epsilon \lesssim 11$)⁸ has been uncovered

as very interesting for solid particle suspensions, as it is characterized by a powerful combination of spontaneous charge dissociation and the possibility of much longer screening lengths than in water.^{5,6,10,11}

Recently, we discovered that the low-polar regime may well be as important for emulsions, due to electrostatic effects that are mostly induced by the difference in the dielectric constant between the two liquids.^{12,13} For instance, in our initial experiments the water phase spontaneously acquired a charge due to ‘preferential ion partitioning’ (see ‘Results and discussion’), giving rise to charge-stabilized, additive-free, water-in-oil emulsions. For particle-stabilized (so-called ‘Pickering’¹⁴) emulsions, we found that image charge effects can bind even extremely hydrophobic, nonwetting particles to the oil–water interface. These observations contradict the common belief that all stable emulsions require emulsifiers and that partial wetting of the particles is essential for their interfacial binding.^{1–3}

Clearly, the various electrostatic effects directly affect the structure and stability of both emulsions and colloidal suspensions. This makes them not only of interest for the production of these particular compounds, but also for the encapsulation of food and drugs,^{15,16} colloidal self-assembly,^{15,17} scientific model studies^{18–20} and microfluidics applications (see also ref. 12). Despite this potentially broad impact, electrostatic effects in emulsions have received little attention before.^{9,18,21,22} Therefore, in the present report we investigate both experimentally and theoretically the role of electrostatics in oil–water mixtures in more detail; a study that was initiated in ref. 12 and 13.

^a Soft Condensed Matter, Debye Institute, Utrecht University, Princetonplein 5, 3584 CC Utrecht, The Netherlands. E-mail: m.e.leunissen@nyu.edu, a.vanblaaderen@phys.uu.nl

^b Institute for Theoretical Physics, Utrecht University, Leuvenlaan 4, 3584 CE Utrecht, The Netherlands. E-mail: j.w.zwanikken@phys.uu.nl, r.vanroij@phys.uu.nl

^c Princeton Institute for the Science and Technology of Materials, and Department of Physics, Princeton University, Princeton, NJ 08534, USA

[†] Present address: Center for Soft Matter Research, New York University, 4 Washington Place, New York, NY 10003, USA. m.e.leunissen@nyu.edu, chaikin@nyu.edu.

In particular, we will focus on the generality and tunability of the ion partitioning process and its associated structural phenomena in particle-containing oil–water mixtures. We will also take a closer look at the nature and tunability of the interactions between the particles that get trapped at the oil–water interface, forming two-dimensional crystals. We stress, however, that the ‘out-of-plane’ structure of the colloidal suspension, perpendicular to the oil–water interface, will be our main focus. Since a pioneering study by Pieranski,¹⁹ a lot of attention has been devoted to the in-plane structure and particle interactions of the colloidal layer at the interface, but the out-of-plane structure has largely gone unstudied.

The present combination of experiments and theory provides a deeper understanding of the electrostatic interactions between oil–water emulsions and colloids and will open the way to additional levels of control in the manipulation of these and related systems.

Experimental

Suspensions

We used polymethylmethacrylate (PMMA, density $\rho_{\text{PMMA}} \approx 1.19 \text{ g ml}^{-1}$) spheres, made by dispersion polymerization, sterically stabilized with covalently bound poly(12-hydroxystearic acid) and covalently labeled with the fluorophore rhodamine isothiocyanate (RITC).²³ After the synthesis, we washed the particles extensively with hexane (p.a., Merck) and petroleum ether (p.a., Merck) to remove any unreacted species. The particle radius was $1.08 \mu\text{m}$, with a polydispersity of 3%, as determined by static and dynamic light scattering. We dispersed the dry particles in the index matching organic solvent cyclohexyl bromide (CHB, $\rho_{\text{CHB}} = 1.33 \text{ g ml}^{-1}$, $\geq 99\%$, Fluka) or in a nearly index- and density-matched mixture of CHB and 27.2% *cis*-decalin by weight ($\rho_{\text{decalin}} = 0.89 \text{ g ml}^{-1}$, 99%, Sigma-Aldrich). The *cis*-decalin was used as received, while the CHB was used either as received or after washing with deionized water and drying with CaCl_2 powder (anhydrous, $\geq 95\%$, Baker).

Microscopy samples

All samples were confined to glass capillaries of $0.1 \times 1.0 \text{ mm}$ inner dimensions (VitroCom), before studying them by confocal scanning laser microscopy (Leica NT or Leica SP2 CSLM).¹² To obtain a large oil–water interface, with its normal perpendicular to gravity, we filled half of the length of the $\sim 5 \text{ cm}$ long capillaries with the oily suspension and the other half with the water phase. For smaller interfaces, oriented with their normal parallel to gravity, we rinsed the capillary with the water phase, which left behind droplets on the walls, and then filled it with the particle suspension. In some cases, we added NaCl ($\geq 99\%$, Baker) or tetrabutylammonium bromide salt (TBAB, $\geq 99\%$, Fluka) to the water phase. We did this by first preparing a saturated solution and then diluting this to the desired concentration. The addition of TBAB to the CHB phase was done in a similar way. In one case, we replaced the water phase with glycerol ($\geq 99\%$, Sigma-Aldrich), following the same procedures for sample preparation.

Electrokinetic characterization

To estimate the Debye screening length of the oily CHB (/decalin) phase we measured its conductivity with a model 627 Scientifica instrument and translated this value into an ionic strength using Walden’s rule, as we described before.^{6,12} The viscosities of the CHB solvent and the CHB–decalin mixture were 2.269 and 2.217 mPa s, respectively (measured at $25 \text{ }^\circ\text{C}$ with a Schott ViscoSystem), while the dielectric constant was 7.9 for the pure CHB²⁴ and 5.6 for the mixture. The latter value was determined through correlation with the measured refractive indices of several mixtures and the pure CHB and *cis*-decalin solvents.²⁵

To get an idea of the extent of ion transport between the oily phase and the water (or glycerol) phase we exposed 50 ml of CHB (/decalin) for 24 h to an equal volume of the other phase and measured the conductivity of the oily phase both before and after. We used these bulk values to estimate the ionic strength of the samples in our microscopy cells, which unfortunately were too small to allow for a direct measurement of the conductivity inside (see also ref. 12).

We determined the magnitude of the particle charge and the sign of the charge at the water–oil interface by means of electrophoresis, as described in ref. 12.

Theory

Connected aqueous and oily salt reservoirs

We start our analysis by first considering two separated salt reservoirs with monovalent ions at concentrations $\rho_{\pm,i}$ in a medium of dielectric constant ϵ_i , where $i = w, o$ is short for the water and oil reservoir, respectively. Without a colloidal component in the reservoirs, $\rho_{+,i} = \rho_{-,i} \equiv \rho_{s,i}$ for neutrality reasons. The Debye screening lengths κ_i^{-1} are given by

$$\kappa_i^2 = \frac{4\pi\beta e^2}{\epsilon_i} 2\rho_{s,i}$$

where $\beta = 1/k_{\text{B}}T$, with k_{B} the Boltzmann constant and T the absolute temperature, and e the elementary charge. We now assume that the two reservoirs are in diffusive equilibrium, such that the chemical potentials $\mu_{\pm,i}$ of the cations and anions in the reservoirs satisfy $\mu_{\pm,o} = \mu_{\pm,w}$. We write:

$$\mu_{\pm,i} = k_{\text{B}}T \ln \rho_{s,i} + \frac{e^2}{2\epsilon_i a_{\pm}} \pm e\psi_i$$

where the second term on the right hand side is the electrostatic self-energy of the ions, which depends on the ion radius a_{\pm} , and where the third term is due to an average electrostatic potential ψ_i in reservoir i . We can now consider the linear combination $\mu_{+,o} + \mu_{-,o} = \mu_{+,w} + \mu_{-,w}$ in order to eliminate the potentials, thus obtaining

$$\ln \rho_{s,w}^2 + \frac{e^2}{2\epsilon_w a_+} + \frac{e^2}{2\epsilon_w a_-} = \ln \rho_{s,o}^2 + \frac{e^2}{2\epsilon_o a_+} + \frac{e^2}{2\epsilon_o a_-}$$

from which we conclude that $\rho_{s,o}$ can easily be many orders of magnitude smaller than $\rho_{s,w}$ if $\epsilon_o \leq 15$, for typical sub-nanometer ionic radii. As a consequence, the Debye screening length in oil can be much larger than that of water, by three orders of magnitude. By considering the linear combination

$\mu_{+,o} - \mu_{-,o} = \mu_{+,w} - \mu_{-,w}$ we eliminate the ionic densities and find

$$\frac{e^2}{2\varepsilon_w a_+} - \frac{e^2}{2\varepsilon_w a_-} + \psi_w = \frac{e^2}{2\varepsilon_o a_+} - \frac{e^2}{2\varepsilon_o a_-} + \psi_o$$

from which we conclude that a nonvanishing electrostatic potential difference $\Psi_w - \Psi_o$ exists for cases where the ionic radii of the cations and anions are different.

We point out that this primitive model of solvation, involving a simple expression for the solvation chemical potential, is sufficient for the present purpose of revealing the interesting effects and the main mechanisms at work. A detailed quantitative comparison with the experiments will require a more sophisticated solvation model though, such as that given by the molecular theory of solvation.²⁶

Poisson–Boltzmann theory

We now consider a planar interface between oil and water in the presence of (hydrophobic) colloidal particles, like we have in our experiments. We denote the distance from the interface by x ; the water phase resides at $x < 0$ and the oil phase at $x > 0$. We imagine the water phase to be in osmotic contact with the water reservoir discussed above, and the oil phase with the oil reservoir. We are now interested in the ionic density profiles $\rho_{\pm}(x)$, which we assume to be described by a Boltzmann distribution:

$$\rho_{\pm}(x) = \rho_{s,i} \exp(\pm \beta e(\psi(x) - \psi_i)) \quad (1)$$

where $\Psi(x)$ is the yet unknown self-consistent electrostatic potential, $\rho_{s,i}$ the ion density and Ψ_i the potential in the reservoirs.

The density profile of the colloidal particles, $\rho(x)$, involves (i) electrostatics, because the colloids are charged, (ii) the Carnahan–Starling excess chemical potential to describe hard-core packing effects (of the colloids only), and (iii) an external potential $V(x)$ that characterizes their hydrophobicity.¹³ The latter is described through the colloid–water and colloid–oil surface tensions, for which we assume $\gamma_{cw} = 10 \text{ mN m}^{-1}$ and $\gamma_{co} = 1 \text{ mN m}^{-1}$, respectively. Then, following Pieranski’s geometric argument,¹⁹ a colloidal particle of radius a with its center at $x \in (-a, a)$ is subject to the external potential

$$V(x) = 2\pi a^2(\gamma_{cw} - \gamma_{co})\left(1 - \frac{x}{a}\right) - \pi a^2 \gamma_{wo} \left(1 - \frac{x^2}{a^2}\right)$$

where $\gamma_{wo} = 9.2 \text{ mN m}^{-1}$ is the assumed surface tension of the oil–water interface.[‡] Similarly, a particle completely immersed in water, *i.e.* $x < -a$, has $V(x) = 4\pi a^2(\gamma_{cw} - \gamma_{co}) \approx 10^6 k_B T$ for $a \approx 1 \mu\text{m}$, and a particle completely immersed in oil, *i.e.* $x > a$, has $V(x) = 0$. The potential $V(x)$ has a deep minimum at $x = x^* = a(\gamma_{cw} - \gamma_{co})/\gamma_{wo} \equiv a \cos \theta$, with θ the wetting angle, provided that $|\gamma_{cw} - \gamma_{co}| < \gamma_{wo}$. Otherwise, $V(x)$ is monotonic and we speak of non-wetting. In the calculations presented here we will assume a small degree of wetting, $\theta \approx 168^\circ$, such that $V(x^*) \approx -10^3 k_B T$ and $V(x < 0)$ is so large that $\rho(x) \approx 0$

[‡] Note that we shifted the potential of ref. 19 by an arbitrary constant for convenience.

in the water phase, reflecting the strongly hydrophobic character of our colloids.

If we take into account all the different contributions mentioned above then the corresponding Boltzmann distribution reads:

$$\eta(x) = \eta_i \exp(-\beta V(x) - \beta \mu(\bar{\eta}) - Z \beta e(\psi(x) - \psi_i)) \quad (2)$$

where $\eta = 4\pi a^3 \rho/3$ is the colloidal packing fraction, $\bar{\eta}$ is a weighted packing fraction (see below) and $Z = 450$ is the particle charge, while η_i is set by the imposed colloid density far from the interface. The set of equations for the unknown profiles $\rho_{\pm}(x)$, $\rho(x)$, and $\Psi(x)$, eqn (1) and (2), can be closed by the Poisson equation:

$$\beta e \frac{d^2 \psi(x)}{dx^2} = \kappa_i^2 \sinh \beta e(\psi(x) - \psi_i) - \frac{4\pi \beta e^2}{\varepsilon_i} Z \rho(x) \quad (3)$$

Donnan equilibrium and boundary conditions

Eqns (1)–(3) form a closed set and can be solved numerically, once the boundary conditions are specified. If we fix the colloid density in the bulk oil phase to $\lim_{x \rightarrow \infty} \rho(x) = \rho_b$, then electroneutrality dictates that the Donnan potential in the oil phase, $\Psi(\infty)$, satisfies

$$\sinh \beta e \left(\lim_{x \rightarrow \infty} \beta(\psi(x) - \psi_o) \right) = \frac{Z \rho_b}{2 \rho_{s,o}}$$

while in the water phase $\lim_{x \rightarrow -\infty} \psi(x) = \psi_w$, which follows also from eqn (3) with $\rho(-\infty) \approx 0$. Further conditions are the continuity of the electric displacement field at the interface,

$$\lim_{x \downarrow 0} \varepsilon_w \frac{d\psi(x)}{dx} = \lim_{x \uparrow 0} \varepsilon_o \frac{d\psi(x)}{dx}$$

and no electric fields in the bulk phases,

$$\lim_{x \rightarrow \pm \infty} \frac{d\psi(x)}{dx} = 0$$

Non-local density approach

In eqns (2) and (3), we treated the charge and packing fraction of the colloids ‘locally’: a number density of colloids $\rho(x)$ at x was connected to a charge density $Z\rho(x)$ at x , thereby concentrating the charge of the colloids to their center. This relatively simple approach can be improved by distributing the colloidal charge such that a colloid centered at x contributes to the charge distribution in the interval $x \in (x - a, x + a)$. One can write:

$$\overline{Z\rho(x)} = \int_{x-a}^{x+a} dx' Z\rho(x') w_c(|x - x'|)$$

where we take the weight function $w_c(h) = (2a)^{-1}$, proportional to the corresponding colloidal surface area at a distance h from the center. The weight function is a constant, since the surface area of a sphere between h and $h + \Delta h$ is $2\pi a^2 \Delta h$, independent of the height. In a similar way, we treat the

packing fraction

$$\bar{\eta}(x) = \int_{x-2a}^{x+2a} dx \eta(x) w_p(|x-x'|)$$

where $w_p(h) = (12a^2 - 3h^2)/32a^3$, taken from ref. 27. The non-local treatment of the charge density avoids artificial screening effects between the interface and the colloids close to the interface, while the non-local treatment of η assures a physical maximum to the packing fraction. For more technical details we refer to ref. 13.

Results and discussion

Ion partitioning and its associated phenomena are general

In ref. 12, we showed how mixtures of the low-polar, oily organic solvent cyclohexyl bromide (CHB) and water can be dominated by strong, long-ranged electrostatic effects, mainly due to the difference in the dielectric constant between the two phases ($\epsilon_{\text{CHB}} = 7.9$ and $\epsilon_{\text{water}} \approx 80$ at 25 °C). Especially in mixtures where we added hydrophobic polymethylmethacrylate (PMMA) particles to the oil phase a variety of electrostatic phenomena showed up readily. Among the observations were a net positive charge and a dense particle layer at the water–oil interface, a large zone (50–100 μm) depleted of particles immediately next to the interface and a body-centered-cubic Coulomb, or ‘Wigner’, crystal with lattice constants up to 40 μm , further away in the oil phase.

We attributed these phenomena to (preferential) partitioning of the micro-ions between the water and oil phases. Namely, if one considers the electrostatic self-energy, $e^2/2\epsilon_i a_{\pm}$, of a monovalent ion in solution, it is clear that ions from the oil phase should strongly partition into the higher dielectric constant water phase (see also the Theory section). Moreover, strong specific interactions, such as hydrogen bonding, enhance the affinity for water even further.^{26,28,29} Differences in the solvation free energies of different ions then cause unequal partitioning, or ‘preferential’ absorption, of certain ionic species, leading to a net charge of the water phase. That this (preferential) partitioning process can indeed have a pronounced effect on the structure of emulsions and colloids has recently been confirmed by the theoretical studies of Zwanikken and van Roij.¹³

Ion partitioning is not specific to the water–CHB couple, but should be a general phenomenon, occurring as soon as there is a difference in the dielectric constant between the two liquid phases (one can easily understand this by equating the electrochemical potentials in the two phases; see the Theory section). To illustrate this, we performed an experiment in which we exchanged the water phase for glycerol ($\epsilon_{\text{glycerol}} = 42.5$ at 25 °C). As can be seen in Fig. 1, a sharp interface forms when glycerol is brought into contact with a suspension of PMMA particles ($a = 1.08 \mu\text{m}$) in CHB/decalin (a solvent mixture that nearly matches the refractive index and density of the particles; $\epsilon_{\text{CHB/decalin}} \approx 5.6$, see the Experimental section). Moreover, the overall appearance of the sample is very similar to that seen for PMMA–CHB/decalin suspensions in contact



Fig. 1 Confocal micrograph of PMMA spheres (radius 1.08 μm) suspended in CHB/decalin ($\epsilon \approx 5.6$), in contact with glycerol ($\epsilon \approx 42.5$). Notice the particle monolayer, followed by a large zone depleted of particles near the glycerol–suspension interface (oriented perpendicular to the plane of the image), as well as the body-centered cubic colloidal crystal with a large lattice constant in the bulk oil phase. Due to the curvature of the (2D) interface several particle rows of the dense-packed monolayer are visible simultaneously, giving it a somewhat broader appearance. The direction of gravity (g) is indicated in the top-left corner.

with water (compare, for instance, with the results in ref. 12 or the results for a water interface presented further below).

The most notable feature is perhaps the 97 μm wide zone entirely depleted of particles, that separates the bulk colloidal Coulomb crystal from the interface. Interestingly, observations of the direction of electrophoretic motion of freely floating glycerol droplets in CHB/decalin show that the glycerol phase carries a positive charge; the same sign as the charge on the colloids, for which we found that $Z \approx +450$ from electrophoretic mobility measurements. The positive charge of the glycerol phase is due to preferential absorption of H^+ ions from the oil phase, which, together with Br^- , originate from the partial dissociation of the HBr decomposition product of CHB. Of the ionic species known to be present, H^+ is bound to have the strongest affinity for glycerol, because its glycerol solvation free energy will contain a large hydrogen-bonding contribution, which is unlikely to be counterbalanced by the ion–solvent interactions in the oily CHB/decalin phase. Besides, solvated H^+ likely has a smaller ionic radius than Br^- , if one takes the measured radii in water as an indication: $a_{\text{H}^+} = 0.28 \text{ nm}$ and $a_{\text{Br}^-} = 0.33 \text{ nm}$ ³⁰ (the importance of the ionic radii in the preferential partitioning process follows directly from the equation for the electrostatic self-energy given above). In short: the spontaneous charging of the glycerol phase leads to Coulombic repulsion of the colloidal particles in the oil phase, thereby giving rise to the observed depletion effect (in ref. 12 we estimated that a moderate potential of 100 mV would suffice for this).

At shorter distances from the interface, the particles experience an attraction to their opposite image charge in the higher dielectric constant glycerol phase, and get permanently trapped at the interface. Before, we demonstrated the existence of this kind of attraction for an oil–water system, by means of optical tweezers experiments.¹² Importantly, the particles that are bound by image charge attraction do not contribute significantly to the repulsion that causes the depleted zone, because their charge is almost entirely cancelled by the image charge in the glycerol phase. In fact, the particle’s own countercharge constitutes the image charge: when a charged colloid approaches the interface, the counterions get absorbed

by the higher dielectric constant liquid, due to the ions' aversion to the oil phase. As a result, the 'stripped' oppositely charged colloids are attracted and bind to the interface. Our theoretical calculations indicate, though, that the image charge attraction may not be strong enough to account for the high density of the interfacial colloidal layer that is often seen in our experiments, because the electrostatic repulsion between the interfacial particles increases with the coverage. Possibly, in-plane correlations between the colloids, a lower particle charge at the interface due to charge regulation, or a small degree of wetting of the otherwise very hydrophobic particles (see ref. 12) could explain the high density.

In connection with this, it is interesting to note that Zwanikken and van Roij¹³ found that one can also get a depleted zone without preferential ion partitioning, in the case that the particles are strongly bound to the interface by wetting effects. In this case, the depleted zone is due to a *partial* deformation of the usual double-layer structure around the colloids in the vicinity of the interface. Qualitatively: the strong wetting-induced binding leads to a very dense layer of colloids, but now not all of their counterions go to the higher dielectric constant phase, because the system can lower its free energy by partially screening the electrostatic repulsions between the densely packed interfacial particles in the oil phase. Consequently, the charge of the colloidal monolayer is only partially compensated for by the countercharge in the higher dielectric constant phase, leading to a repulsion of the colloids in the bulk oil phase. Note that a similar effect would occur without wetting if the image charge attraction is strong enough to overcome the interparticle repulsions, giving a sufficiently dense colloidal layer at the interface.

In our experiments, the depleted zone is likely caused by a combination of bulk charge repulsion due to preferential ion partitioning and colloidal monolayer repulsion due to double layer deformation. As an illustration, we calculated the distribution of the micro-ions and the colloids near the glycerol-CHB/decalin interface, using the (estimated) parameters from the experiment in Fig. 1 ($a_+ = 0.28$ nm, $a_- = 0.33$ nm, $Z = 450$ and $\kappa_o^{-1} = 3.6$ μm , see below). Our mean-field Poisson-Boltzmann approach, as outlined in the Theory section, captures the preferential ion partitioning, the double layer deformation, the image charge attraction and any wetting effects. Unfortunately, at present we do not know how large the respective contributions of image charge attraction and possible wetting effects exactly are in our experiments (see above). Therefore, we will simply assume that $\theta \approx 168^\circ$, in order to obtain a clear demonstration of the effect of double layer deformation. This choice should give rise to a strong adsorption of the colloids at the interface, because the associated binding energy is very large $|V(x^*)| \gtrsim 10^3 k_B T$. The estimated image charge binding energy is significant as well, easily exceeding $10^2 k_B T$ for sufficiently long screening lengths, $\kappa_o a < 0.5$, as is the case in our experiments.

Fig. 2 shows the results of the calculation. First of all, from the inset it is clear that one indeed gets a dense layer of colloids at the glycerol-oil interface, followed by a region that is entirely depleted of particles. These results are in qualitative agreement with the experimental observations, but the extent of the depleted zone is underestimated, probably because the

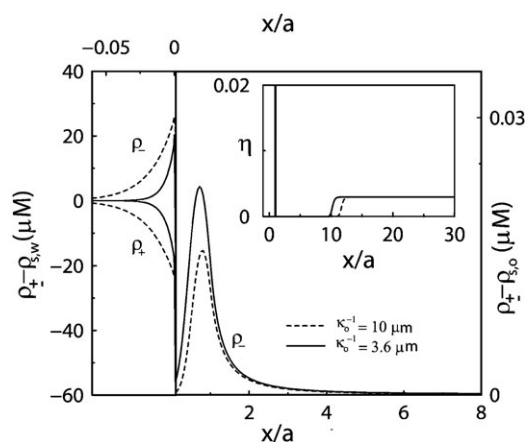


Fig. 2 The calculated distribution of negative (ρ_-) and positive (ρ_+) micro-ions around the glycerol-CHB/decalin interface (at $x = 0$) and the packing fraction of colloidal particles near the interface (inset). We used $a_+ = 0.8a_- = 0.28$ nm, $\eta = 0.003$, $\epsilon_o = 5.6$ and $Z = 450$, together with $\kappa_o^{-1} = 3.6$ μm , as in the experiments (solid lines), and $\kappa_o^{-1} = 10$ μm (dashed lines). In both cases the ρ_+ profiles nearly coincide with the x -axis for $x > 0$ ($\ll 10^{-3}$ μm). Note that the x -axis has a different scale below and above $x = 0$, and that the distances are scaled by the particle radius, $a = 1.08$ μm . We subtracted the salt concentration in the water reservoir on the left y -axis and the salt concentration in the oil reservoir on the right y -axis to make the charge separation at the interface clearly visible.

Poisson-Boltzmann theory does not take into account the colloid-colloid correlations, leading to an overestimate of the pressure exerted by the bulk crystal. Moreover, the predicted bulk charging due to preferential ion partitioning may be too low, because we only included the electrostatic self-energies of the ions and no other contributions like, for instance, hydrogen bonding effects (see above; a detailed quantitative comparison with the experiments will require a more sophisticated solvation model, such as that given by the molecular theory of solvation²⁶). Looking at the micro-ion profiles, we do not only see a large partitioning-induced density difference across the glycerol-oil interface, but also a clear charge separation due to a highly asymmetric distribution of the screening ions around the interfacial colloidal layer. A considerable fraction of the countercharge is concentrated in a thin layer inside the glycerol phase, close to the interface.

For comparison, we also calculated the distributions for a system with a longer Debye screening length, $\kappa_o^{-1} = 10$ μm . In this case, the double layer is even more deformed, with a large fraction of the counterions of the interfacial colloidal layer inside the glycerol phase. Nevertheless, the depleted zone is seen to increase, as compared to the previous case. This is mostly due to the increase in screening length of the oil phase. From our calculations, we find that the fraction of screening ions in the glycerol phase increases rapidly when $\kappa_o a < 1$, and that it becomes more than 50% around $\kappa_o a \approx 0.1$. Note that in the very small $\kappa_o a$ limit essentially all the countercharge will reside inside the glycerol phase, causing the depleted zone to shrink again, because the absorbed countercharge will largely cancel the charge of the interfacial colloidal layer. In this case, only the bulk charge repulsion due to preferential ion partitioning will remain.

Table 1 Bulk measurements of ion partitioning in mixtures of low- and high-polar solvents (in order of appearance in the text). σ_{start} is the conductivity of the low-polar phase before contact with the high-polar phase; σ_{final} is the conductivity of the low-polar phase after 24 h exposure to the high-polar phase

Low-polar phase	High-polar phase	$\sigma_{\text{start}}/\text{pS cm}^{-1}$	$\sigma_{\text{final}}/\text{pS cm}^{-1}$
CHB	Glycerol	6760	975
CHB	Water	6760	700
Chloroform	Water	4000	1760
CHB	Water–NaCl (6 M)	6470	580
CHB	Water	6470	478
CHB–TBAB	Water	15 320	3210
CHB	Water–TBAB (2 M)	6760	>20 000

To conclude this section, we show that the occurrence of pronounced micro-ion partitioning from the oil phase into the higher dielectric constant glycerol phase is also confirmed by our bulk conductivity measurements on as received CHB, before and after 24 h of exposure to an equal volume of glycerol (see the Experimental section). In this time, the conductivity (σ) was seen to drop from 6760 to 975 pS cm⁻¹ (Table 1). For the microscopy sample in Fig. 1 we used a purified CHB/decalin mixture, which at the start of the experiment had a bulk conductivity of 220 pS cm⁻¹. We estimate that the ion scavenging activity of glycerol would eventually bring this down to $\sigma \approx 30$ pS cm⁻¹ or less, which corresponds to a Debye screening length $\kappa_0^{-1} \gtrsim 3.6$ μm . This large screening length gives rise to long-ranged repulsions between the charged colloids in the oil phase, which explains the relatively large lattice spacing ($l = 9.8$ μm) of the colloidal crystal far away from the interface \S . Finally, we point out that our claim that ion partitioning is a generally occurring process is further supported by still other experiments, including studies in which we replaced the oily phase with another solvent, while maintaining the water phase. For instance, when chloroform ($\epsilon_{\text{chloroform}} = 4.7$ at 25 $^\circ\text{C}$) was exposed to water, its conductivity was seen to drop from 4000 to 1760 pS cm⁻¹ (Table 1).

Time-dependence of the partitioning process and its associated phenomena

While in ref. 12 we only considered the final, fully equilibrated state of our microscopy samples, we will take here a more detailed look at their evolution over time, starting from the initial stages shortly after preparation. In particular, we will focus on the time scale of the ion transport process and the development of the associated structural signatures, like the depleted zone and the colloidal Wigner crystal.

Fig. 3 shows the interface between an oily colloidal suspension of PMMA particles in purified CHB/decalin and water, 10 min after preparation ($t = 0$, Fig. 3a) and 6 h later (Fig. 3b). Clearly, during this time both the depleted zone and the spacing in the crystal expanded. At $t = 0$ the bulk of the crystal had a lattice spacing $l = 7.7$ μm and it started ~ 46 μm from the interface, while 6 h later the depleted zone extended over 111 μm before giving way to a crystal with $l = 15$ μm .

\S We assume that the particles interact with a screened Coulomb pair potential⁴⁰: $V(r) = \frac{Z^2 e^2}{\epsilon_0 (1 + \kappa_0 a)^2} \frac{\exp[-\kappa_0 (r - 2a)]}{r}$ with r being the interparticle distance.

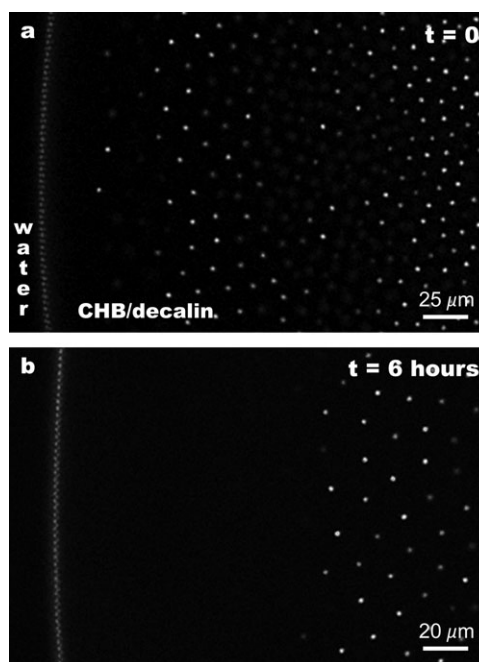


Fig. 3 The interface between a suspension of PMMA particles in CHB/decalin ($\epsilon \approx 5.6$) and water ($\epsilon \approx 80$), 10 min after preparation ($t = 0$) (a) and 6 h later (b).

From 6 h onwards, the depleted zone and the crystal near the water–oil interface (within a distance of a few millimeters) were seen not to change much anymore, but the equilibration of the entire length of the colloidal suspension (typically 2–2.5 cm) took one or more days, as indicated by the growing lattice constant. These observations are in accordance with ongoing ion scavenging by the water phase. From a comparison with bulk conductivity measurements (Table 1), we expect the screening length inside the microscopy sample cell to increase from $\kappa_0^{-1} \approx 1.4$ μm to $\kappa_0^{-1} \approx 4.6$ μm . The theoretical results in Fig. 4 show that for our experimental parameters such a change in the screening length will indeed cause an expansion of the depleted zone, although the actual extent is underestimated again (see the previous section). Moreover, electrophoretic measurements on free-floating water droplets in CHB/decalin indicate that the water phase developed a net positive charge.

The slowly spreading ‘ionic absorption front’ is readily visible in the image of Fig. 3a, which was taken shortly after preparation. While the bulk crystal far from the interface (right side of the image) at that time still had a lattice constant of 7.7 μm , close to the interface the spacing had already grown to 12 μm , without a deterioration of the crystalline order. Taking the screened Coulomb potential and the estimated values for the screening length given above, we find an interaction energy of 1.6 $k_B T$ between two neighboring particles in the bulk crystal at $t = 0$ and 5.4 $k_B T$ after 6 h \P . Thus, the increased screening length is responsible for a higher interaction energy, and thereby for the observed enhancement of the crystalline order at later times, despite the larger

\P Here we assume that the particle charge is constant. Note, however, that under certain conditions this is not necessarily the case.⁴¹

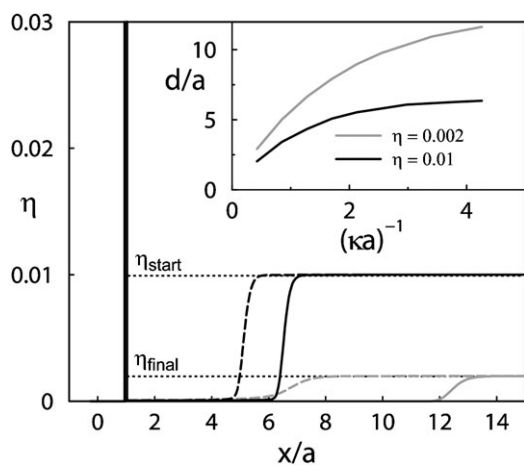


Fig. 4 The calculated packing fraction of colloidal particles near the water-CHB/decalin interface (at $x = 0$) and the extent of the depleted zone (d) as a function of the Debye screening length in the oily phase (inset). Note that all distances (x , d , κ) are scaled by the particle radius, $a = 1.08 \mu\text{m}$. The dashed profiles correspond to the experimental conditions immediately after sample preparation ($\kappa_0^{-1} = 1.4 \mu\text{m}$), while the solid lines are the conditions found after equilibration ($\kappa_0^{-1} = 4.6 \mu\text{m}$). We used two different overall packing fractions, $\eta = 0.01$ (black) and $\eta = 0.002$ (gray), and set $a_+ = 0.8a_- = 0.28 \text{ nm}$, $\epsilon_0 = 5.6$ and $Z = 450$, as in the experiments. The dotted lines indicate the experimentally observed packing fractions of the bulk crystal at $t = 0$ (η_{start}) and 6 h later (η_{final} , Fig. 3).

interparticle spacing. The observed time scale of hours to days for the ion partitioning process is consistent with diffusion of the micro-ions towards and across the interface (taking, for instance, a typical diffusion constant of $3.3 \times 10^{-10} \text{ m}^2 \text{ s}^{-1}$ for an ion with a radius $a_{\pm} = 0.3 \text{ nm}$ ³⁰).

We point out that in the final, fully equilibrated state the crystal should have the same lattice spacing throughout. Obviously, in our experiments the final crystal with its inflated lattice spacing will contain fewer particles than the starting suspension. For instance, in Fig. 3 we prepared the suspension at $\eta = 0.010$, but in the final crystal the packing density was only $\eta = 0.002$. Naturally, a certain fraction of the particles ends up in the colloidal layer at the interface, but this can not explain the big decrease in packing fraction. Apparently, the particles that are not accommodated in the crystal or at the water-oil interface were forced towards the sample cell walls, as the wall coverage was seen to increase over time. This intriguing observation requires further investigation, because at present it is not clear what causes the enhanced adsorption of the particles at the wall. Note that Fig. 4 suggests that the lower final packing density in our sample actually leads to a larger depleted zone.

Tuning the charge at the interface

The net charge that the water phase acquires depends on the final oil-water distribution of all the positive and negative ionic species that are present. In ref. 12 we demonstrated how one can tune the charge at the water-CHB interface through the pH, because H^+ and OH^- are among the major ionic species present. Interestingly, the recent theoretical investigations by Zwanikken and van Roij¹³ clearly showed that it is

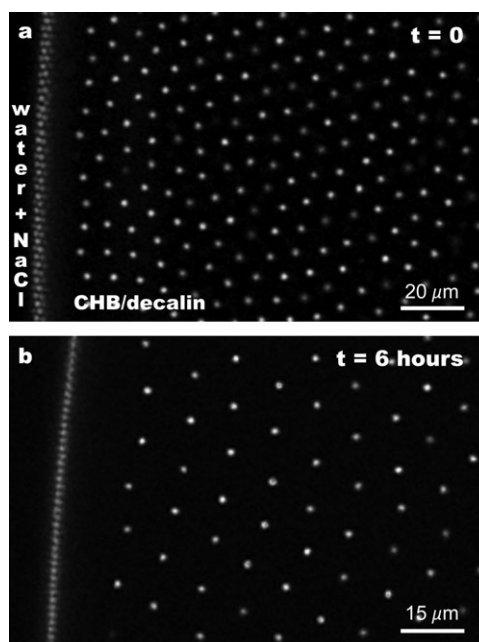


Fig. 5 The interface between a suspension of PMMA particles in CHB/decalin and water with 3.0 M NaCl, 10 min after preparation ($t = 0$) (a) and 6 h later (b).

not necessarily the pH (H^+/OH^- concentration) that controls the droplet charge. Instead, they found that any ionic species has the potential to do so, depending on how it distributes between the oil and water phases. To confirm this experimentally, we looked at the effect that NaCl has when it is added to the water phase.

In Fig. 5, we dissolved 3.0 M NaCl in the water and again created an interface with a suspension of PMMA particles in CHB/decalin. Fig. 5a shows the sample 10 min after preparation ($t = 0$) and Fig. 5b is the same sample 6 h later. Interestingly, whereas the lattice spacing of the crystal was seen to increase quite dramatically, from $6.7 \mu\text{m}$ initially to $13.2 \mu\text{m}$ after 6 h, the depleted zone did not grow very big, only $19 \mu\text{m}$. Bulk conductivity measurements, as well as the large lattice spacing of the final crystal, indicate that the presence of NaCl did not stop the ion flux from the oil to the water phase, though. For instance, when as received CHB with $\sigma = 6470 \text{ pS cm}^{-1}$ was exposed to water saturated with NaCl the conductivity was seen to drop to 580 pS cm^{-1} , which is comparable to the effect obtained with deionized water ($\sigma_{\text{final}} = 478 \text{ pS cm}^{-1}$, Table 1). From this, we conclude that it is likely not so much the different final screening length in the oil phase that causes the shrinkage of the depleted zone (as compared to the sample with pure water), but the change in the partitioning-induced bulk charge of the water phase.

This conclusion is supported by the results in Fig. 6, where we calculate the extent d of the depleted zone as a function of the ratio between the radii of the major cationic and anionic species present in the system (see the Theory section). More specifically, we set $a_+ = 0.3 \text{ nm}$ as the radius of a typical cation and varied a_- for the anion. In our experiments, H^+ and OH^- are the major ionic species in the case of pure water, and then $a_-/a_+ = 1.2$; for NaCl $a_-/a_+ = 0.9$. Although we do not find quantitative agreement with the experimental observations,

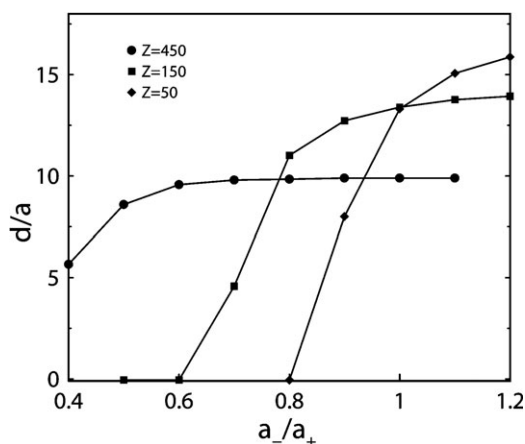


Fig. 6 The calculated extent of the depleted zone, d , as a function of the anion radius a_- and the particle charge Z . We fix the other parameters to be $a_+ = 0.3$ nm, $\epsilon_0 = 5.6$, $\kappa_0^{-1} = 4.6$ μm , $\eta = 0.003$ and $a = 1.08$ μm , which is comparable to the experimental values.

the qualitative trend is the same, especially when we assume a lower particle charge, $Z = 50$]. From Fig. 6, it can be seen that with a decreasing a_-/a_+ ratio also the extent of the depleted zone decreases, just like we observe when we add NaCl to the water phase. This behavior is due to reduced positive charging of the water phase. In fact, from electrophoresis measurements we find that the water droplets with 3.0 M NaCl actually carry a small negative charge.

If we only take into account the electrostatic self-energies of the ions, one would expect that preferential ion partitioning results in a negative charge of the high dielectric constant phase when $a_-/a_+ \lesssim 1.0$ (see the Theory section). In our case, the negative charge will already develop at somewhat larger ratios, though, because the deformed double layers of the colloids at the interface add extra anions to the water phase. Obviously, a net negative charge of the water phase will counteract the repulsion by the interfacial colloidal layer, reducing the depleted zone, while a positive bulk charge will increase the depleted zone. However, from Fig. 6 it appears that for the latter case the extent of the depleted zone saturates with increasing a_-/a_+ ratio. This asymptotic behavior can be explained within the framework of charge renormalization:^{31,32} if the ‘contact’ potential $\Psi(a)$ of the colloidal monolayer in the oil phase exceeds several $k_B T/e$, then the counterions will condense onto the colloidal surfaces, thereby essentially compensating any sufficiently high water charge. The larger maximum width of the depleted zone at lower particle charge, as seen in Fig. 6, is due to the lower contact potential and the lower osmotic pressure of the bulk crystal. We find, for the present parameters, that the contact potential is at most $\Psi(a) \approx 6 k_B T/e$.

|| In general, we find better quantitative agreement between our theoretical calculations and the experiments when we assume a smaller particle charge. This is in accordance with earlier observations that for highly correlated systems the Poisson–Boltzmann theory corresponds better to more advanced theoretical approaches and Monte Carlo computer simulations if one assumes a lower charge.⁴² Moreover, we did not consider possible charge regulation of the colloids, which could lower their charge at the interface.

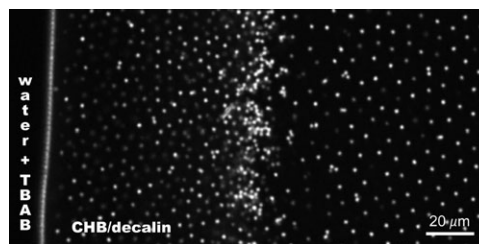


Fig. 7 The interface between a suspension of PMMA particles in CHB/decalin and water with 186 mM tetrabutylammonium bromide (TBAB) salt, a couple of minutes after preparation.

From our experiments and the theoretical predictions it is clear that the final equilibrium state of the water–oil sample depends on the dissociation and partitioning equilibria of all ionic species present. The fact that these equilibria for different ionic species are coupled to each other makes the picture even more complicated (*e.g.*, H^+ can pair up with both OH^- and Br^-). Moreover, one has to keep in mind that the ions do not only migrate from the oil to the water phase, but can pass the interface in both directions. The latter becomes immediately clear when one performs conductivity measurements in the presence of tetrabutylammonium bromide salt (TBAB), to take an extreme case as an example. TBAB is frequently used as a phase transfer catalyst,³³ because of its ability to dissolve in both water (saturation concentration ~ 2 M) and organic solvents, like CHB (saturation at ~ 300 μM ⁵). Its moderate solubility in low-polar solvents is due to the relatively large, organic cation ($a_{\text{TBA}^+} = 0.54$ nm in water³⁰). When we dissolved a small amount of TBAB in CHB (as received), so that $\sigma = 15\,320$ pS cm^{-1} , and exposed this to deionized water, the conductivity dropped to 3210 pS cm^{-1} (Table 1). Thus, there was a net ion flux towards the water phase, just like we saw before with pure CHB and water. In the ‘reverse’ experiment we exposed CHB (as received) with $\sigma = 6760$ pS cm^{-1} to water saturated with TBAB. In this case, the conductivity of the CHB went off-scale ($> 20\,000$ pS cm^{-1}). Apparently, there now was a large net flux of ions towards the CHB phase.

Fig. 7 shows visual proof for the occurrence of ion transport from the water to the oil phase, as well as the possible effects associated with it. Shown is the interface between a PMMA–CHB/decalin suspension and water with 186 mM TBAB, a couple of minutes after preparation. What one should know first of all, is that the colloids can reverse their charge when the TBAB concentration in the oil phase is sufficiently high (a few tens of μM , depending on the particle concentration).^{6,10} We hypothesize that this is the reason for the band of aggregates that is visible at ~ 85 μm from the interface. It separates the ‘original’, positive particles from the ones that have reversed their charge, and thus roughly indicates how far the TBAB had diffused into the oil phase at that time. Of course, not only the particle charge changes, but also the screening length, which becomes shorter as the ions diffuse in. Therefore, it is no surprise that we now find a colloidal fluid close to the interface, while further away there is a crystal, with a lattice constant that is likely still the same as at the start of the experiment ($l = 7.8$ μm , compared for instance with the crystal in Fig. 3a, which had a similar spacing at the start of the experiment).

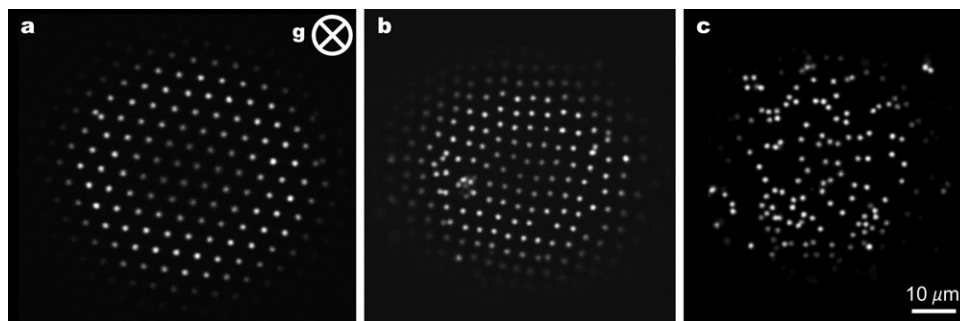


Fig. 8 Confocal microscopy images of PMMA particles permanently bound at the interface of hemispherical water droplets on the sample cell wall (as seen from the oil phase) in (a) pure CHB ($\epsilon = 7.9$), (b) CHB with a low concentration of tetrabutylammonium bromide (TBAB) salt, and (c) CHB with a high TBAB concentration. The scale bar is the same for all images and the direction of gravity (g) is indicated.

Nature of the interfacial particle interactions

Finally, we turn our attention to the colloidal particles that are bound to the water–oil interface. First of all, we point out that although surface tension effects will often play an important role in the binding of interfacial particles, we demonstrated in ref. 12 that image charge attraction alone can be strong enough to enable the permanent binding of non-wetting particles to like-charged oil–water interfaces. Thus, image charge attraction forms an essential ingredient in the full understanding of particle-stabilized emulsions.

In our experimental system, the interfacial particles form a dense monolayer (e.g. Fig. 3) or a non-close-packed, two-dimensional surface crystal (Fig. 8a) with hexagonal symmetry, depending on the particle concentration in the bulk suspension. Apparently, at low coverage densities strong electrostatic repulsion between the interfacial particles leads to a large lattice spacing. Pieranski pointed out that charged colloids at a water–oil interface can experience a long-ranged repulsion due to an effective dipole–dipole interaction.¹⁹ This interaction is due to the asymmetry of the double layer around the interfacial particle, which induces a dipole normal to the oil–water interface.^{19,34–37} However, Aveyard *et al.* demonstrated that this repulsion is not strong and long-ranged enough to give rise to the kind of surface crystals seen here.³⁸ Using optical tweezers, they quantified the repulsive interaction potential between charged polystyrene particles, trapped at the interface between an alkane mixture and water.¹⁸ Based on these measurements, they postulated that the repulsion primarily arises due to charge–charge interactions through the oil phase, as a result of a small charge at the particle–oil interface.

Although for a somewhat different experimental system, the results in Fig. 8 strongly support this latter hypothesis. Shown are the surfaces of a series of hemispherical water droplets on the sample cell wall, surrounded by a dilute suspension of PMMA particles in CHB. The fairly good CHB-solubility of TBAB salt (see above) allowed us to change the interfacial particles' electrostatic interactions through the oil phase in a very direct way; to the best of our knowledge this has not been demonstrated before. Thus, in Fig. 8a we used CHB without any added salt and the estimated screening length $\kappa_o^{-1} \approx 940$ nm, in Fig. 8b CHB with a low concentration of TBAB such that $\kappa_o^{-1} \approx 190$ nm, and in Fig. 8c a higher TBAB

concentration, resulting in $\kappa_o^{-1} < 135$ nm (note that these estimates are based on bulk conductivity measurements; likely the actual ionic strength near the water droplet is lower). From this series, it is clear that increased screening in the oil phase causes the surface crystal to melt into a (two-dimensional) colloidal fluid. Likely, this effect was enhanced by a simultaneous decrease of the particle charge, because in Fig. 8c some of the particles had reversed their charge and were attracted to the other particles (these plus–minus attractions do not yet occur at the lower TBAB concentration of Fig. 8b).

To make sure that the observed melting transition was not the result of increased screening in the water phase—due to partitioning of the TBAB salt—we repeated the experiment with droplets of NaCl saturated water. Even at this high salt concentration, the appearance of the droplets remained the same as that of deionized water droplets, giving nice surface crystals in the presence of pure CHB (similar to the one shown in Fig. 8a). Apparently, the repulsion between the interfacial particles does not (strongly) depend on the screening length inside the water phase. This observation makes possible dipole–dipole interactions between partially wetted particles unlikely as a primary source of the strong interparticle repulsion, as those interactions should decrease strongly when the ionic strength of the water phase is increased.³⁴ Taken together with the fact that the PMMA particles carry a significant charge when dispersed in CHB ($Z \approx +450$), we believe the present observations to be strong evidence that the large lattice spacing of the surface crystals is due to long-ranged Coulomb repulsion through the oil phase only.

Conclusions

We have studied in more detail the pronounced electrostatic effects of which we recently discovered that they can make an important contribution to the interactions in mixtures of low- and high-polar liquids, like oil–water emulsions. Combining experiments and theory, we here developed a better understanding of the interactions and structure in oil–water emulsions that contain colloidal particles. On the one hand, the new insights reveal possible pitfalls in the production of stable (Pickering) emulsions, like repulsive interactions between the interface and the stabilizing species which could be easily overlooked. On the other hand, however, they offer new means

to control the system, for instance through a judicious choice of the ionic species that are present. We believe that our observations are of general importance, because we found that most of the electrostatic effects in our water/oil-particle mixtures are due to (preferential) partitioning of the microions between the two liquid phases. As evidenced by our theory and experiments, this partitioning process is a general phenomenon, which occurs as soon as there is a difference in the dielectric constant between the two liquids.

The ongoing ion scavenging by the high-polar phase sets the time scale for the development of the characteristic structural features, which typically evolve over hours to days. On a qualitative level, the observed colloidal structure normal to the water–oil interface agrees well with our theoretical calculations, which predict a partial deformation of the colloidal double layer in combination with a spontaneous charging of the water phase (in future work, better quantitative agreement can likely be achieved by using a more sophisticated molecular solvation model and by correcting for strong correlations within the framework of the Poisson–Boltzmann theory). Experimentally, we have demonstrated that the final net charge of the water phase depends on the dissociation and partitioning equilibria of all ionic species present. Moreover, we showed that one should be aware of the fact that the ions do not only diffuse from the low-polar phase to the (energetically more favorable) high-polar phase, but that they can also cross the interface in the opposite direction in order to obtain a chemical potential balance. In addition, we demonstrated that the colloidal ‘surface crystals’ at the interface are due to long-ranged repulsive Coulomb interactions through the oil phase only, which can be manipulated through the addition of an oil-soluble salt. To conclude, we point out that the novel insights presented here will not only be of interest for the production of Pickering and charge-stabilized emulsions,^{1,3,14,39} but also for the encapsulation of food, drugs and cosmetics,^{15–17} as well as colloidal (self-)assembly^{15,17} and microfluidics applications.

Acknowledgements

We thank D. Derks for particle synthesis and A. D. Hollingsworth for solvent characterization and useful discussions. This work was supported by the Stichting voor Fundamenteel Onderzoek der Materie, the Nederlandse Organisatie voor Wetenschappelijk Onderzoek (The Netherlands), The National Aeronautics and Space Administration, and the National Science Foundation (USA).

References

- 1 P. Becher, *Emulsions: theory and practice*, Krieger, New York, 1977.
- 2 *Modern aspects of emulsion science*, ed. B. P. Binks, The Royal Society of Chemistry, Cambridge, 1998.
- 3 R. Aveyard, B. P. Binks and J. H. Clint, *Adv. Colloid Interface Sci.*, 2003, **100–102**, 503–546.
- 4 W. B. Russel, D. A. Saville and W. R. Schowalter, *Colloidal Dispersions*, Cambridge University Press, Cambridge, 1999.
- 5 A. Yethiraj and A. van Blaaderen, *Nature*, 2003, **421**, 513–517.

- 6 C. P. Royall, M. E. Leunissen and A. van Blaaderen, *J. Phys.: Condens. Matter*, 2003, **15**, S3581–S3596.
- 7 M. F. Hsu, E. R. Dufresne and D. A. Weitz, *Langmuir*, 2005, **21**, 4881–4887.
- 8 P. C. van der Hoeven and J. Lyklema, *Adv. Colloid Interface Sci.*, 1992, **42**, 205–277.
- 9 W. Ryoo, S. E. Webber, R. T. Bonnecaze and K. P. Johnston, *Langmuir*, 2006, **22**, 1006–1015.
- 10 M. E. Leunissen, C. G. Christova, A.-P. Hynninen, C. P. Royall, A. I. Campbell, A. Imhof, M. Dijkstra, R. van Roij and A. van Blaaderen, *Nature*, 2005, **437**, 235–240.
- 11 E. V. Shevchenko, D. V. Talapin, N. A. Kotov, S. O’Brien and C. B. Murray, *Nature*, 2006, **439**, 55–59.
- 12 M. E. Leunissen, A. van Blaaderen, A. D. Hollingsworth, M. T. Sullivan and P. M. Chaikin, *Proc. Natl. Acad. Sci. U. S. A.*, 2007, **104**, 2585–2590.
- 13 J. Zwanikken and R. van Roij, *Phys. Rev. Lett.*, cond-mat/0705.2327, accepted.
- 14 S. U. Pickering, *J. Chem. Soc., Trans.*, 1907, **91**, 2001–2021.
- 15 M. F. Hsu, M. G. Nikolaides, A. D. Dinsmore, A. R. Bausch, V. D. Gordon, X. Chen, J. W. Hutchinson, D. A. Weitz and M. Marquez, *Langmuir*, 2005, **21**, 2963–2970.
- 16 B. F. Gibbs, S. Kermasha, I. Alli and C. N. Mulligan, *Int. J. Food Sci. Nutr.*, 1999, **50**, 213–224.
- 17 O. D. Velev, K. Furusawa and K. Nagayama, *Langmuir*, 1996, **12**, 2374–2384.
- 18 R. Aveyard, B. P. Binks, J. H. Clint, P. D. J. Fletcher, T. S. Horozov, B. Neumann, V. N. Paunov, J. Annesley, S. W. Botchway, D. Nees, A. W. Parker, A. D. Ward and A. N. Burgess, *Phys. Rev. Lett.*, 2002, **88**, 246102–246101.
- 19 P. Pieranski, *Phys. Rev. Lett.*, 1980, **45**, 569–572.
- 20 P. Lipowsky, M. J. Bowick, J. H. Meinke, D. R. Nelson and A. R. Bausch, *Nat. Mater.*, 2005, **4**, 407–411.
- 21 K. D. Danov, P. A. Kralchevsky, K. P. Ananthapadmanabhan and A. Lips, *Langmuir*, 2006, **22**, 106–115.
- 22 R. Ellis, *Z. Phys. Chem.*, 1912, **80**, 597–616.
- 23 G. Bosma, C. Pathmamanoharan, E. H. A. de Hoog, W. K. Kegel, A. van Blaaderen and H. N. W. Lekkerkerker, *J. Colloid Interface Sci.*, 2002, **245**, 292–300.
- 24 W. M. Heston, E. J. Hennelly and C. P. Smyth, *J. Am. Chem. Soc.*, 1950, **72**, 2071–2075.
- 25 M. E. Leunissen, PhD Thesis, Utrecht University, 2007, <http://www.colloid.nl>.
- 26 *Molecular Theory of Solvation*, ed. F. Hirata, Kluwer Academic Publishers, Dordrecht, 2003.
- 27 P. Tarazona, U. Marini Bettolo Marconi and R. Evans, *Mol. Phys.*, 1987, **60**, 573.
- 28 Y. Marcus, *Ion Solvation*, Wiley, Chichester, UK, 1985.
- 29 J. Lyklema, *Fundamentals of Interface and Colloid Science*, Academic Press, London, UK, 1995.
- 30 A. G. Volkov, D. W. Deamer, D. L. Tanelian and V. S. Markin, *Liquid Interfaces in Chemistry and Biology*, Wiley, New York, 1998.
- 31 S. Alexander, P. M. Chaikin, P. Grant, G. J. Morales, P. Pincus and D. Hone, *J. Chem. Phys.*, 1984, **80**, 5776–5781.
- 32 E. Trizac, L. Bocquet and M. Aubouy, *Phys. Rev. Lett.*, 2002, **89**, 248301.
- 33 C. M. Starks, C. L. Liotta and M. Halpern, *Phase-transfer catalysis*, Chapman & Hall, New York, 1994.
- 34 F. H. Stillinger, *J. Chem. Phys.*, 1961, **35**, 1584–1589.
- 35 A. J. Hurd, *J. Phys. A: Math. Gen.*, 1985, **18**, L1055–L1060.
- 36 J. C. Earnshaw, *J. Phys. D: Appl. Phys.*, 1986, **19**, 1863.
- 37 D. Goulding and J. P. Hansen, *Mol. Phys.*, 1998, **95**, 649–655.
- 38 R. Aveyard, J. H. Clint, D. Nees and V. N. Paunov, *Langmuir*, 2000, **16**, 1969.
- 39 B. P. Binks, *Curr. Opin. Colloid Interface Sci.*, 2002, **7**, 21–41.
- 40 E. J. Verwey and J. T. Overbeek, *Theory of the stability of lyophobic colloids*, Elsevier, New York, 1948.
- 41 C. P. Royall, M. E. Leunissen, A.-P. Hynninen, M. Dijkstra and A. van Blaaderen, *J. Chem. Phys.*, 2006, **124**, 244706.
- 42 A. Torres, A. Cuetos, M. Dijkstra and R. van Roij, *Phys. Rev. E*, 2007, **75**, 041405.